Fuel 289 (2021) 119833

Contents lists available at ScienceDirect

Fuel

journal homepage: www.elsevier.com/locate/fuel

Full Length Article

Quantitative characterisations of spray deposited liquid films and post-injection discharge on diesel injectors

Dan Sykes [a], Jack Turner [a], Viacheslav Stetsyuk [a], Guillaume de Sercey [a], Martin Gold [b], Richard Pearson [b], Cyril Crua [a,*]

[a] Advanced Engineering Centre, University of Brighton, Brighton, UK
[b] BP International Ltd., Pangbourne, UK

ARTICLE INFO

Keywords:
Injector deposit
Dribble
Cavitation
Rarefaction
Liquid film
High-speed microscopy

ABSTRACT

Transient injection phases have been identified as a prominent source of inefficiencies and exhaust gas constituents detrimental to both public health and the environment. The rapid reduction of in-nozzle flow rate at the end of diesel injection events inhibits spray atomisation and releases large slow-moving liquid structures into the cylinder. This uncontrolled release of fuel results in wetting of the nozzle surface through rogue droplets diverting back towards the nozzle. The resulting films create fuel-rich regions that may later get drawn into the exhaust, contributing to engine-out emissions. They also present an ideal environment for reactions with combustion products and adherence of deposit precursors. Despite recent experimental advances there is a lack of quantitative data relating the operating conditions to the quantity of fuel deposited on nozzle orifices.

To improve our understanding of the underlying near-nozzle and surface-bound processes, we applied high-speed optical microscopy under conditions relevant to passenger vehicles. Image processing techniques were used to quantify the deposition of fuel films and their spreading with time. A single component fuel (n-dodecane) was injected using an injector instrumented with a thermocouple to measure the sub-surface nozzle tip temperature. Injection duration, timing and pressure were varied to reveal their influence on the deposition and overspill of fuel onto the nozzle.

We conclude by presenting an analysis of the film behaviour as function of injection pressure, in-cylinder pressure and bulk gas temperature. Relative to the conditions investigated, spray wetting was more pronounced at the reduced load conditions.

1. Introduction

The climate crisis is compounded by the imminent depletion of fossil fuel supplies, forcing governments to invoke successions of increasingly stringent vehicle emission regulations [1]. The considerable pressure for a fast-paced engine evolution is further intensified by the consumer expectation of a continual linear progression in vehicle performance, vehicle size and improved fuel economy. It is well understood that the primary sources of inefficiencies and hazardous exhaust gas constituents, reside in the combustion dynamics and preceding air-fuel mixing processes [2,3]. The properties of the fuel sprays, i.e. the shape of the jet, entrainment of hot gasses and breakup of the individual liquid structures, governs the vapour region encompassing the jets [4,5]. Auto-ignition is initiated by several sites throughout the vapour head, rapidly spreading throughout the gaseous fuel region, promoting vaporisation of neighbouring fuel structures [4]. The vaporised fuel is broken down releasing its energy whilst governing the production of soot [5,6]. The presence of localised fuel rich regions, in addition to overly lean zones, inhibits vaporisation and the subsequent reactions [7]. Incomplete combustion products have the capacity to get drawn into the exhaust, potentially passing through the aftertreatment system and directly contributing towards Unburnt Hydrocarbon (UHC) emissions [8].

Complex fuel designs and precise, highly calibrated injector geometries are of prime importance in the pursuit of enhanced gas-fuel mixing [9], eliciting a fast paced evolution in Fuel Injection Equipment (FIE) [10]. Atomisation is enhanced through greater Injection Pressure (IP), with some diesel systems reaching 300 MPa and Gasoline Direct Injection (GDI) systems reaching 50 MPa [10]. New injector designs incorporate more orifices with smaller diameters, microscopic flow channels and tighter tolerances, leading to refined jet characteristics [11–14].

* Corresponding author.
E-mail address: c.crua@brighton.ac.uk (C. Crua).

https://doi.org/10.1016/j.fuel.2020.119833
Received 7 August 2020; Received in revised form 12 October 2020; Accepted 20 November 2020

However, fuel degradation may occur through high pressure and thermal pumping loads [15], whilst the compact geometries heighten susceptibility to seizure and blockages from internal deposits [16,17]. The impact of Air to Fuel Ratio (AFR) non-uniformities are also minimised through improved combustion performance when increasing forced aspiration pressures and gas temperatures [18–20]. Yet the severe environmental conditions they induce in the near-nozzle vicinity are thought to further promote formation of detrimental deposits on and within the injector nozzle [21,22].

The accumulation of deposits has been associated with reduced power delivery, engine durability and the production of pollutants [22–26]. In-cylinder deposition may alter an engines autoignition properties through insulation of internal surfaces [27–29], whereas deposit build up on valves may inhibit the airtight sealing and affect valve timing through misalignment [30]. The surfaces of injector nozzles are particularly prone to both fuel films and deposit formation, internally and externally [31,32,21,33]. Severe injector deposits lead to engine failure due to blocking of the orifices/flow channels and needle seizure [34]. Deposits can be found in several locations throughout the FIE with considerable differences in chemical composition and morphology [35–37]. The deposit forming mechanisms are not entirely agreed upon [38], partly due to the great diversity of the cases studied [37]. Nevertheless, it is known that there are important interactions between the nozzle surfaces/pre-existing deposits, nozzle residing fuel and the surrounding conditions (the quenching gas layer encapsulating it in the case of coking) that control deposit formation [38–40]. The surface adhering fuel, primarily attributed to the complex transient injection dynamics [41,42], acts as a mediating component [38].

Modern engines employ multiple injection strategies giving rise to considerably higher frequencies of transient injection phases [43]. The technology is a major breakthrough in the pursuit of reduced NO_X and soot discharge, effectively addressing the NO_X, soot and piston work trade-offs whilst lowering engine noise [44,45]. Despite the clear benefits, the higher number of Start Of Injection (SOI) and End Of Injection (EOI) phases presents a persistent source of surface wetting and emissions [42,46]. It is already known that the early and late phases of the injection produce large, slow moving and often surface-bound liquid structures [47–50], but documented characterisation of these structures is limited. It is likely that these structures are too large to undergo complete combustion, producing detrimental combustion by-products subsequently drawn into the exhaust where they either impede aftertreatment durability or directly contribute towards UHC emissions [51,2,52]. Unburnt fuel remaining in the liquid phase may impinge on nearby surfaces [53], forming films that potentially release vaporised UHCs throughout the cycle [32]. Prolonged film exposure to the in-cylinder environment may promote deposit formation through fuel degradation, adherence of deposit forming precursors and possible catalysation of radical chain reactions [38,54,22]. Consequently, fuel bound to any in-cylinder surface has the potential of causing deposits that adversely affect engine operation [55].

The nozzle residing fuel and near-nozzle conditions are almost entirely dependent on the transient injection regimes, also governing the degradation, phase transition and removal of the films throughout the cycles [56,32]. Several other researchers have looked at characterising both EOI and the subsequent post-injection processes using experimental methods, normally using high pressure vessels or bespoke optical engines under non-reactive conditions [40,56,41,57,58]. Computational fluid dynamics is also regularly employed to predict the flow paths within injectors and overcome the access issues imposed by the severe in-cylinder conditions [59–61,50]. The majority of these studies focus on the dribble event (the fluid dynamics during and immediately after needle re-seating), including the complex fluid behaviour inside the injector nozzle as the sprays collapse. These studies predict the breaking up of the jet into large droplets and ligaments, the volume of atomised fuel and the rapid in-nozzle pressure fluctuations during this period. Despite recent efforts, there is still a lack of quantitative data regarding the fuel film behaviour after the dribble event and the degree of fuel that adheres to the nozzle.

Whilst there are many unexplored fluid dynamic processes occurring at the orifices throughout the full engine cycle [41,39], our investigation is focused on nozzle wetting processes that occur within a few milliseconds of the EOI. Our previous work [39] confirmed that fuel would deposit and spread on the surface of the injector nozzle, both through 'spray wetting' (the impingement of fuel spray droplets back onto the nozzle), and through 'overspill' events (the discharge of nozzle-trapped liquid fuel after the EOI). To better understand and eventually control these phenomena it is essential for us to elucidate their underlying mechanisms. By using a valve covered orifice (VCO) type nozzle and disregarding the orifice connecting cavity of a sac type nozzle, the possible overspill inducing processes were limited to three potential mechanisms (Fig. 1). Overspilling fuel from a VCO-type injector could be caused by: spreading of the liquid fuel out of the orifice by capillary action; expansion of trapped gas through equalisation of pressure with the ambient in-cylinder gas [62]; expansion of the fuel as thermal energy is transferred from the nozzle to the liquid [62]. It should be noted that fuel emergence from a sac type nozzle may have alternate governing processes (purposefully decoupled in this study). Pressure differences between orifice outlets, as caused by high velocity in-cylinder gas, could dislodge the in-sac fuel [39]. The additional cavity within the nozzle provides more space for fuel to reside, potentially accentuating the volume of fuel discharge [63].

The main objectives of this article are to reveal the relative importance of spray wetting and overspill, and to form a detailed account of their dependencies and impact on transient, surface-bound fuel films. We present our development of a quantitative method to measure both the coverage area of surface-bound fuel on the nozzle tip after EOI and the spreading rate, thereby elucidating the underlying mechanism of the initial fuel spreading. The results are explained further using a method to identify the beginning of the overspill events, enabling separation of the spray wetting films from those containing overspilled fuel. In order to decouple the effects of in-cylinder conditions on EOI fuel impingement and overspill, injections were carried out at significantly different timings during the engine cycle, resulting in a range of In-Cylinder Pressures (ICP), ICP gradients, and temperatures. This permitted the investigation of spreading in relation to capillary action and adhesive forces, since the spreading dynamics are a function of both liquid

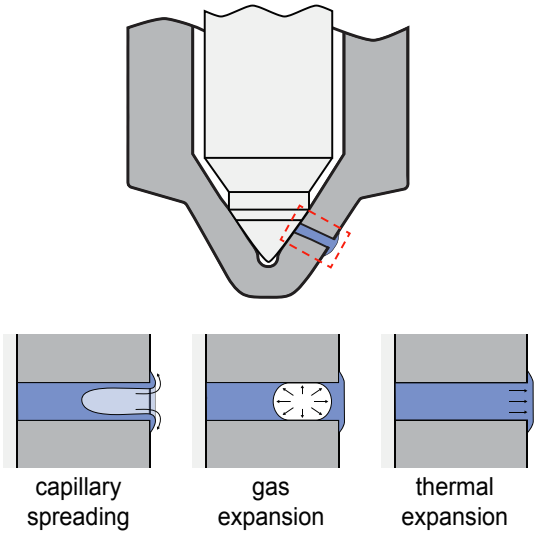

Fig. 1. Schematic of potential mechanisms for the overspill of fuel from the orifices of a VCO nozzle. The overspill could be induced by: spreading of the liquid fuel out of the orifice by capillary action; expansion of trapped gas through equalisation of pressure with the ambient in-cylinder gas; expansion of the fuel as heat is conducted from the nozzle to the liquid.

physical properties and ambient conditions (with the physical properties being a function of both pressure and temperature). We conclude by presenting an analysis of the fuel coverage area and the spreading rate with regards to their dependency on IP, ICP and In-Cylinder Temperature (ICT). The results indicate that surface wetting is more pronounced when injecting smaller fuel mass, relevant towards lower loads and idling.

2. Experimental setup

The experiments were carried out using an optically accessible reciprocating rapid compression machine based around a Ricardo Proteus single cylinder engine (for further information see [64]). A single component fuel surrogate was used (n-dodecane) to enable calculations of physical properties and state. The fuel was delivered by a common-rail system, comprising a high-pressure pump (Delphi DFP-3) rated at 200 MPa, and a six-hole injector (Siemens DW10B) with a VCO type nozzle (Table 1). The injector was instrumented with a K-type thermocouple accurate to ±1 K embedded within the nozzle. The probe tip was positioned next to the orifice enabling temperature measurements just below the nozzle surface. Seventy-five high-speed videos were acquired over fifteen test points with various IPs, injection timings and durations (Table 1). The engine conditions chosen represent low to medium load operation.

The 6-hole instrumented injector was mounted orthogonally to the incident light to allow visualisation of all orifices simultaneously (Fig. 2). The experiments required a high frequency light source (10,000 Hz) and considerable illumination intensities to 'freeze' the motion of the liquid fuel, hence we selected two high-power high-frequency lasers: a solid state diode laser (Cavitar CAVILUX emitting at 690 nm) and a copper vapour laser (emitting at 510.6 and 578.2 nm). The frame exposure of the high-speed camera was set at 1 µs, although the exposure was controlled by the shorter laser pulse durations (Table 2). A schematic of the optical configuration is provided (Fig. 3).

3. Quantification of coverage area and spreading rate

3.1. The image processing algorithm

An image processing algorithm was formulated to semi-automatically extract the coverage area of the liquid films on the nozzle tip. The key processing steps are listed below, visually supplemented with the output image data for each step (Fig. 4):

1. *Normalisation of pixel intensities:* the mean pixel intensity was shifted to correspond to that of the other frames, accounting for small laser pulse-to-pulse variations corresponding to window fouling during testing. The intensity histogram was also stretched in relation to the top and bottom 10% pixel intensities.
2. *Flat fielding:* the illumination across the frame was not homogeneous due to the curvature of the nozzle tip surface offering different scattering angles. The frame intensities were homogenised using a non-linear gradient filter.
3. *Removal of high-frequency noise:* high-frequency noise was removed, and small regions with similar pixel intensity distributions were merged using (un-binarised) morphological closing with a non-flat, disk-shaped structuring element. Followed by morphological opening.
4. *Removal of reflections from the orifice edge:* an elliptical mask layered over the orifice with constant pixel intensities, equal to the mean of those surrounding it, was applied to remove high-intensity reflections from the orifice's edge.
5. *Semi-automatic binarisation:* the mean and spread of pixel intensities across the frame, in conjunction with a user input coefficient, were used for the binarisation threshold. The automatic thresholding performed well, but a user adjustment was required in 33% of the videos to faithfully track the coverage area. These tended to be for higher IP conditions due to increased gas refraction and fuel vapour.
6. *Smoothing of the binarised image:* morphological operators were applied to remove small-scale features related to the nozzle surface topology.

Binarised regions that did not overlap with the orifice were removed, ensuring that any intermittent shadows or abnormal scattering were not mistaken for a fuel film. The fuel coverage area was converted from

Table 1
Operating conditions, hardware parameters & characteristics.

Parameter	Value
Engine speed	500 rpm
Peak motored pressure	5 MPa
Peak motored temperature	650 K
Injection pressure	50; 150 MPa
Injection timing	−30; 0; 30°CA aTDC
Injection duration	0.2; 0.4; 0.6; 1.0 ms
Fuel	n-dodecane
Nozzle type	Siemens DW10B, VCO
Orifice geometry	6 × Ø145 µm holes
K-factor	0.6
Nozzle tip temperature	405 ± 1 K

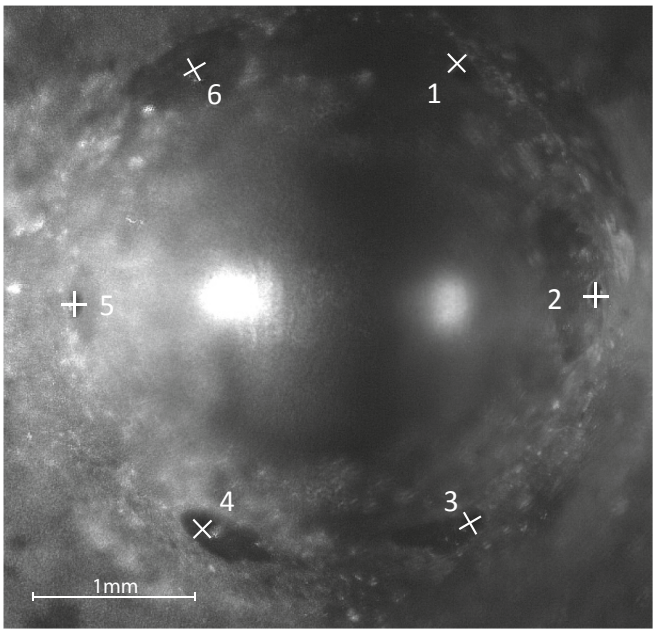

Fig. 2. Video frame showing the injector tip with all orifices in focus. While some orifices show little contrast, orifices 3, 4 and 6 offer satisfactory spatial illumination uniformity, with light from the liquid layers being scattered away from the imaging system, thus making the liquid films appear consistently darker than the dry nozzle surface.

Table 2
Imaging equipment specification.

Parameter	Value
Camera	Phantom V12.1
Frame exposure time	1 µs
Frame rate	10,000 fps
Scale factor	6.58 µm per pixel
Frame resolution	704 × 704 pixels^2
Field of view	4.63 × 4.63 mm^2
Solid state diode laser pulse	25-30 ns (FWHM)
Copper vapour laser pulse	100 µs (FWHM)

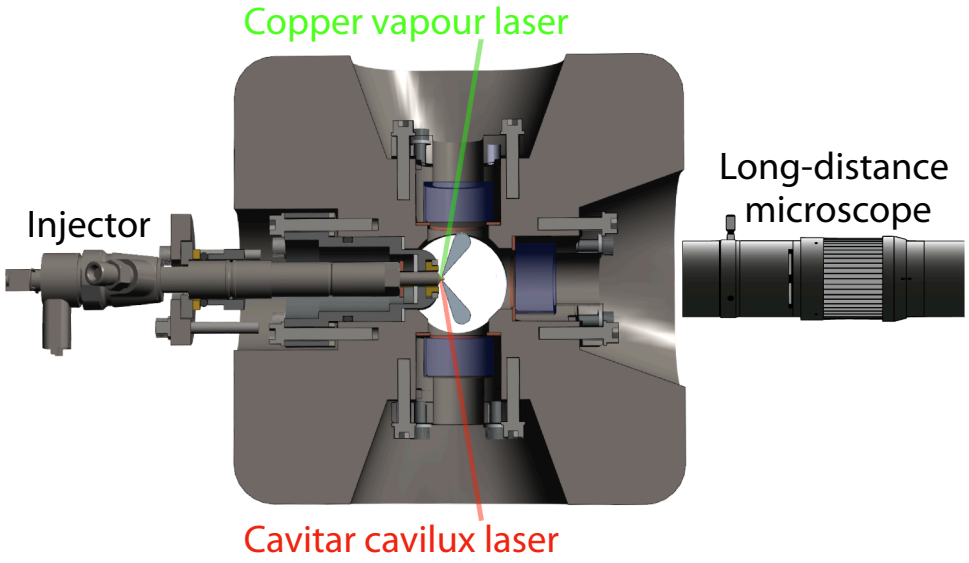

Fig. 3. Schematic of the optical setup used in the experiments. The injector, long distance microscope and camera were position along the same optical axis. The copper vapour and Cavitar cavilux laser beams were transmitted into the cylinder through windows perpendicular to the injector axis, subsequently reflecting from the nozzle surface.

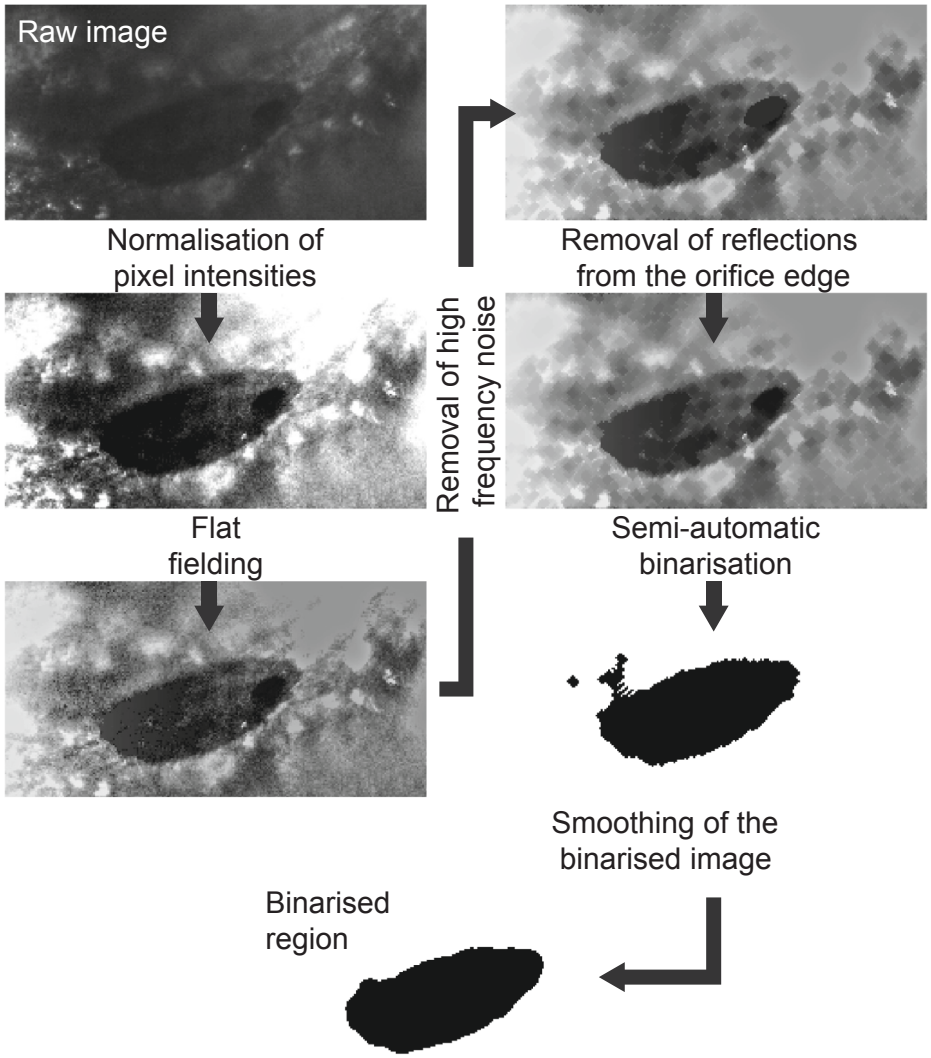

Fig. 4. Flow diagram of the resulting output images from each key processing step. The raw image is processed by the code to obtain a binarised region, subsequently being converted from a pixel count to a film area.

pixels to mm^2 via scaling of the final binarised region, accounting for the 30° inclination of the nozzle tip surface with respect to the optical axis.

The orifice area was removed prior to post processing (Fig. 5) to correctly account for this missing area in the liquid film. A visual inspection of the image processing output was performed for all frames to ensure that the automated measurements accurately tracked the coverage area with time. The recordings which exhibited no fuel film (12% of the dataset) were assigned a value of zero coverage area, included in the statistical analyses. The approach gave consistent results for orifice 3 due to its favourable orientation relative to the illumination source enhancing its spatial uniformity, therefore the image processing was only applied in the area surrounding orifice 3.

The videos were processed between 2 and 6 ms after Start Of Injection trigger (aSOI). Before 2 ms aSOI the light scattering from slow-moving droplets and vapour interfered with the visualisation of the nozzle surface, preventing a reliable view of the fuel films. The films could no longer be quantified after 6 ms aSOI as they spread beyond the field of view. This could have been rectified through the use of a larger field of view, but doing this increased the likelihood of processing errors because of the heterogeneous illumination on the surface outside this region. Hence the processing was performed on the video frames recorded between 2 and 6 ms aSOI with frames every 0.1 ms (frame rate of 10 kHz). Small frame-to-frame errors in coverage area were compensated using a 5-point centred moving average (solid line in Fig. 5). This reduced the impact of any occasional noise, yet decreased the output range to between 2.3 and 5.7 ms, correlating to between 6.9 and 17.1°CA (Crank Angle) after the injection event.

Processing during this time and at this spatial resolution was challenging with severe cases necessitating adjustment of the binarisation threshold or removal of the data (10.7% of total recordings with no clear bias towards particular conditions). The validity of the image processing algorithm was examined through individual inspection of the detected coverage areas. Although the algorithm performed well, occasionally the coverage area was slightly over-estimated as shadows on the nozzle tip were misidentified as part of the film. This form of error is apparent in the supplementary videos and Fig. 6 along the bottom of the red perimeter, highlighted using a yellow dashed line. Visual inspections found that the initial 5 frames gave the largest percentage error relative to the total film area (due to the initial film being small). This enabled us to quantify the worst-case error in our coverage area measurements as ± 0.01 mm^2. An online archive of supplementary videos are provided to demonstrate the performance, highlighting the periods in which the liquid spreading was not calculated.

3.2. Post-processing of the coverage data

Individual temporal coverage area profiles were obtained and averaged for each frame across all videos for each specified operating condition. Images are given for the start, middle and end of the period in which the film area is measured, coupled with the frame averaged measurements when injecting at 50 MPa with 0.6 ms duration (Fig. 7). There is significantly higher spreading towards the left of the orifice due to the direction of in-cylinder gas flow. The evolution of the set-averaged coverage areas with time were found to be linear, with the worst coefficient of determination for the linear fits being 0.87. Hence, the coverage datasets could be represented using the trend line coefficients to permit parametrised comparisons between operating conditions in terms of coverage spreading rate (trend line gradient in mm^2/s) and initial coverage area (y-intercept in mm^2). The two trend line parameters come from the trend line functions, as shown in Fig. 7. The coefficient used for the initial coverage area is taken as the trend line value 2 ms aSOI since the injection duration is up to 1 ms and the dribble duration can take as long as 1 ms. A smaller coefficient of determination was found when using a longer processing period indicating that the overspill, evaporation and bubble emergence occurring later in the cycle causes more significant changes in the spreading rate after 18°CA aSOI, justifying the period chosen for analyses.

3.3. Ascertaining the overspill onset times

Although the coverage area tracking algorithm provided reliable information regarding the surface-bound fluid dynamics in the first 2–6 ms aSOI (6–18°CA aSOI), other important surface wetting phenomena occurred outside this period, identified through visual

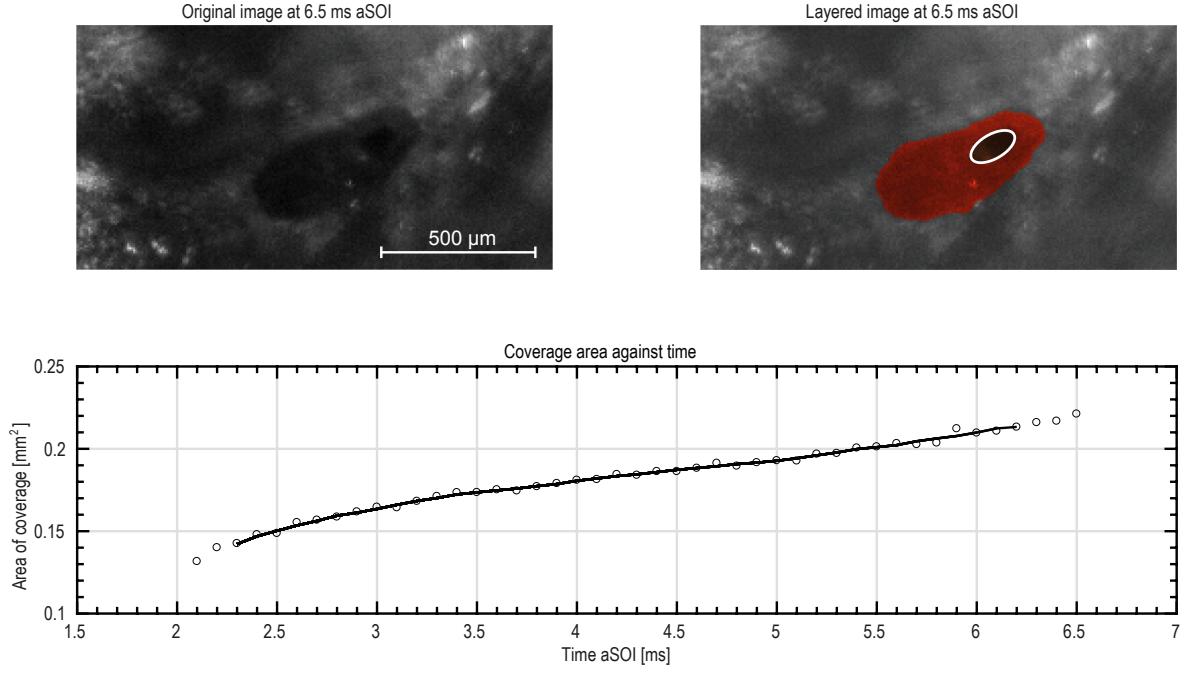

Fig. 5. User interface visually representing the processing output for manual assessment of its performance in real time. The original video frame is displayed (left) along with overlays for the orifice location and wetted area detected by the algorithm (right). The plot represents the detected area in relation to time after start of injection (aSOI) as scatter points, with the 5-point moving average as a solid line.

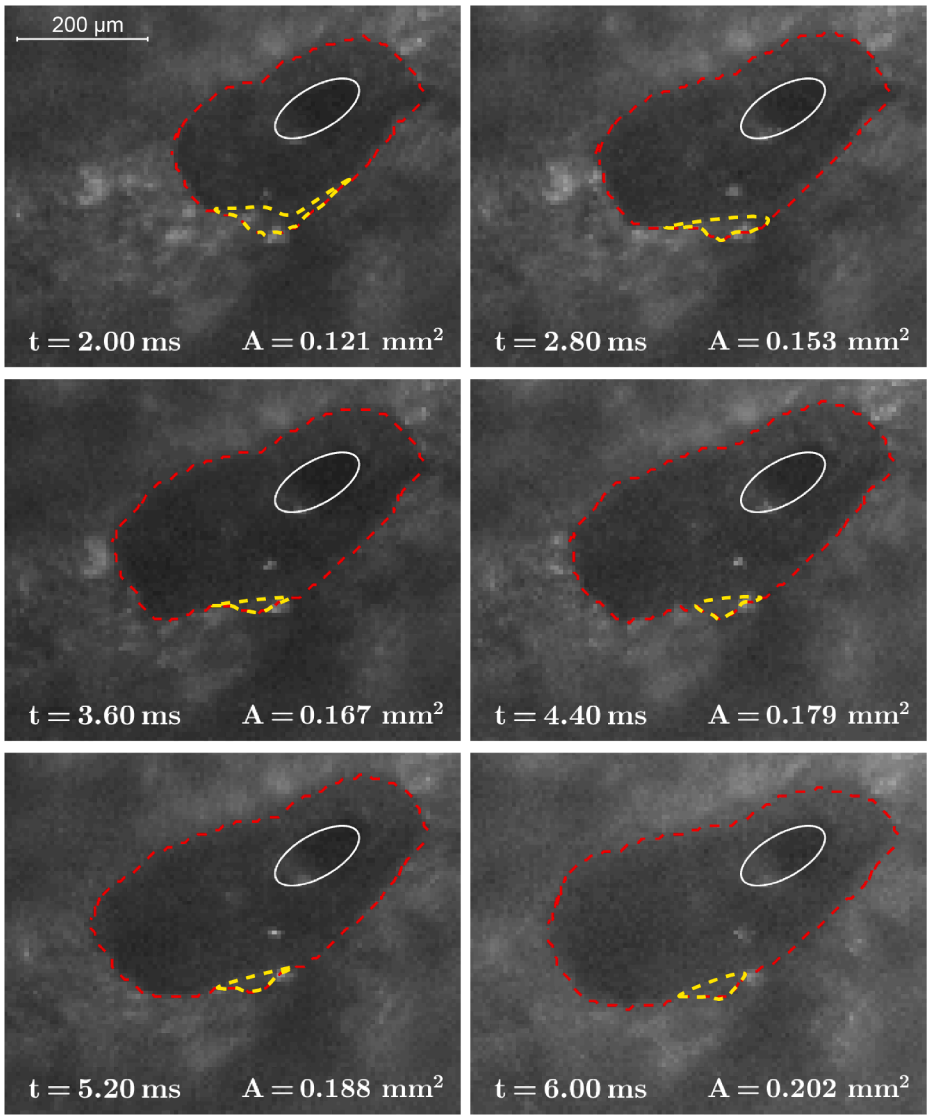

Fig. 6. Video frames cropped around orifice 3 at 50 MPa injection pressure. The detected coverage perimeter is overlaid as a red dashed line and the corresponding detected area (A) displayed on each frame. The yellow dashed line along the bottom of the red perimeter shows the worst-case processing error used to quantify the error in coverage area measurements as ±0.01 mm^2. This sequence is available as Supplementary Video 2, showing the full temporal evolution from the SOI. (For interpretation of the references to colour in this figure legend, the reader is referred to the web version of this article.)

inspection. Evaporation, bubbling, overspill and in-cylinder gas interaction all significantly affect the wetted regions and have specific onset times related to the surrounding conditions [65]. However, the linearity of the temporal film coverage evolutions (discussed in Section 3.2), indicate the aforementioned phenomena are not dominating factors within the period processed. It has already been established that there are two main mechanisms in which fuel can get deposited onto the nozzle surface inducing the films: spray wetting, referring to droplet impingement and fuel adherence at the EOI, and fuel overspilling from the orifices later in the cycle [65]. A video of a typical overspill event is provided in Supplementary Video 1. It is crucial to know if the films quantified through the film tracking algorithm were a mixture of fuel from these two mechanisms or if only the spreading of the initially deposited fuel was accounted for. Furthermore, elucidating the overspill mechanism was a primary aim of the investigation and was shown to be challenging through the film tracking method alone. Thus, a method for quantifying the initial onset of the overspill events was developed.

After the EOI, the orifice exits (visible by the imaging system) are empty permitting the dark internal orifice wall opposing the camera to be seen. When an overspill event begins, the emerging fluid submerges the orifice wall and a high intensity beam reflection from the gas-fluid boundary takes its place, permitting a simple detection method (Fig. 8). The overspill onset times were manually recorded in consideration of this criteria for every orifice in every video for 5 MPa peak ICP, 0.6 ms injection duration at all injection timings tested. The overspill onset times (in terms of crank angle) are analysed for each orifice as well as for all orifices combined (Section 4.1). In the event that fuel did not emerge from an orifice before Bottom Dead Centre (BDC) a timing was not given since fuel vapour and condensation significantly reduced visibility after this point. Consequently, the overspill timing results do not provide any indication on overspill frequency or degree.

4. Results and discussion

4.1. The overspill event

To understand and develop control over the emergence of fuel from the orifices occurring after the injection event (referred to as overspill), it is crucial to elucidate the underlying mechanisms (Supplementary Video 1 depicts a typical overspill event). Establishing the source of the fuel quantified by the film tracking algorithm (being either overspill or spray wetting) is also essential prior to its discussion. By using a VCO-type nozzle and disregarding the orifice connecting cavity of a sac type injector, the possible overspill inducing processes were limited to three potential mechanisms: capillary spreading, thermal expansion and gas expansion (Fig. 1).

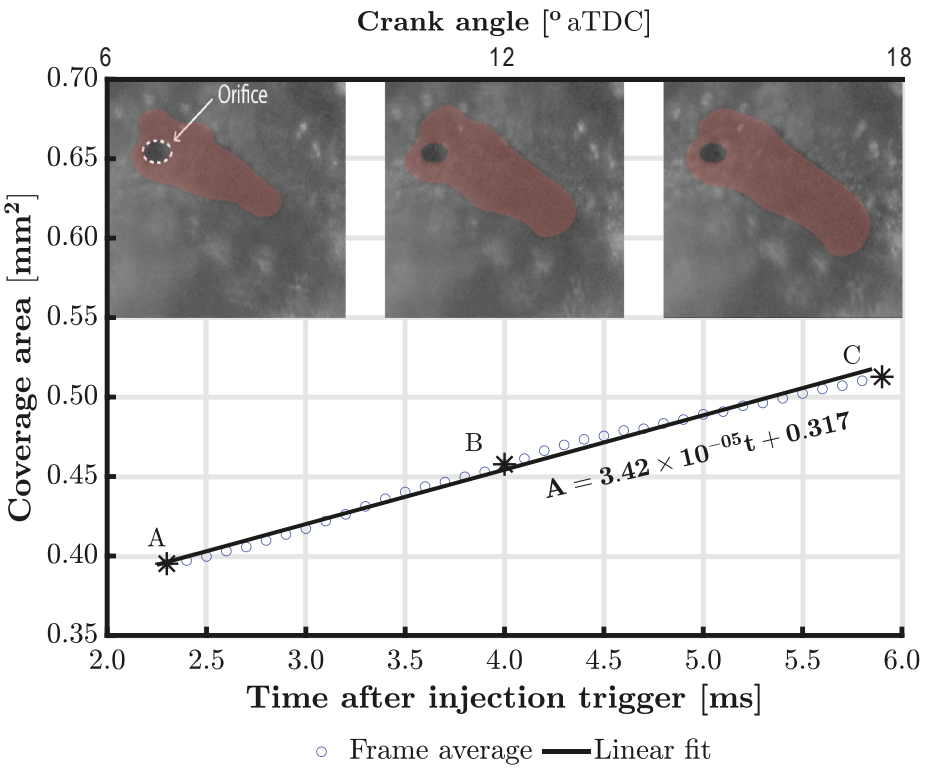

Fig. 7. Linear fitting of a set-averaged coverage trace with regards to time aSOI. The operating conditions were 50 MPa IP, 0.6 ms injection duration and TDC injection timing. Individual points are given by blue circles while the linear fit is shown with a solid black line, its corresponding equation relating coverage area and time is given below. Three images are displayed at the top of the figure that depict representative coverage areas for the start, middle and end of the processing period. (For interpretation of the references to colour in this figure legend, the reader is referred to the web version of this article.)

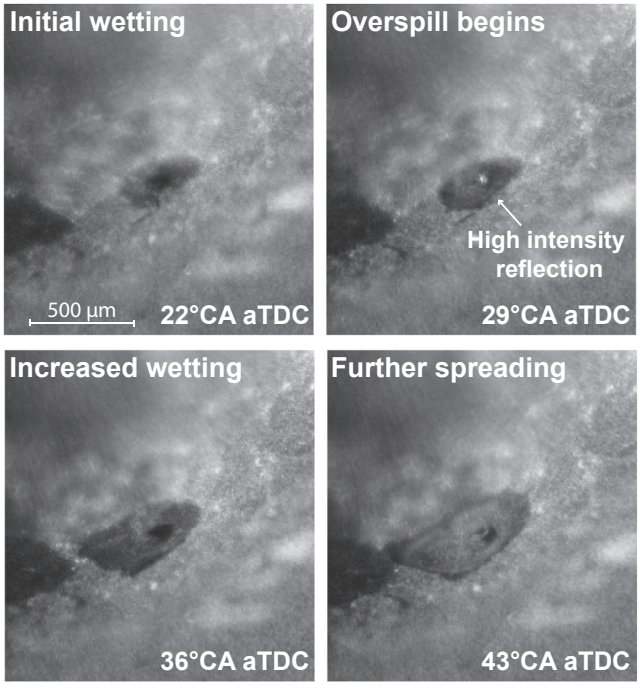

Fig. 8. Four frames giving a chronological account of an overspill event. 22°CA aTDC is prior to an overspill event; at 29°CA aTDC a high intensity reflection of the incident beam appears due to the presence of a liquid interface; 36°CA aTDC onwards depicts a pronounced film spreading due to the amalgamation of overspilt fuel with the pre-existing film. The appearance of the beam reflection is used to manually identify the overspill start timings. A video of a typical overspill event is also provided in Supplementary Video 1.

A key hypothesis investigated was that the presence of gas trapped inside the nozzle orifices could influence the wetting of the VCO nozzle tip during the expansion stroke. As the ICP rapidly drops after Top Dead Centre (TDC), gas trapped within the orifices should expand and displace liquid fuel onto the external surface of the injector. A method for quantifying the time in which these overspilling events begin was adopted and applied to several sets of injections at 50 MPa IP, 0.6 ms duration (Section 3.3). In order to test this hypothesis three injection timings were investigated to produce different pressure gradients after the EOI:

- −30°CA aTDC: during the compression stroke, when the gas pressure rise should inhibit the expansion of trapped gas
- TDC: at top-dead-centre when the motored gas pressure does not vary significantly
- +30°CA aTDC: during the expansion stroke, when the rapid gas pressure drop should promote the expansion of trapped gas.

The overspill onset data shows a much larger delay between injection and overspill when injecting at −30°CA aTDC than for the TDC and 30°CA aTDC injections (Fig. 9). The average onset absolute crank angle for −30°CA aTDC injection timing being even later than for a TDC injection, despite 30°CA timing difference in which the fuel must spend residing within the nozzle. The instantaneous in-cylinder conditions are similar when injecting at ±30°CA injection timing with the primary difference being the opposing ICP differential. Since the largest overspill delays are induced by the −30°CA aTDC injection timing and the shortest by the 30°CA aTDC injection timing, a strong dependency must exist between the overspill and ICP differential. Only one overspill event occurred before TDC and the majority of events for –30 and 0°CA injection timings occurred between 15 and 45°CA aTDC (Fig. 9), when the ICP drop is approaching its maximum (Fig. 13). The clear confirmation of the dependence on a dropping ICP supports the pre-proposed hypothesis: the trapped fuel is forced out of the orifices by gas, equalising with the ICP drop, expanding behind it. The two overspill events beginning just before TDC are likely due to the high density turbulent

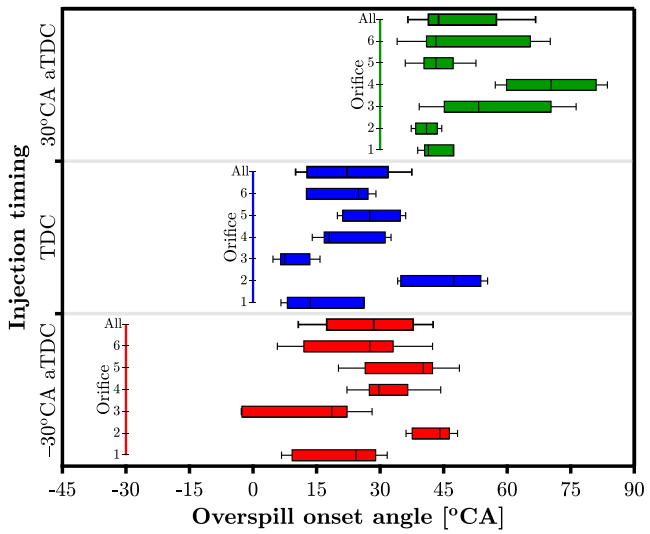

Fig. 9. Box plots for the crank angles in which the overspill events began across three different injection timings; documented for each orifice independently. The line in the centre of the box denotes the average, the box boundaries give the interquartile range and the whiskers show 95 % confidence intervals. The start of injection timing is shown by the vertical coloured lines with TDC given by 0°CA on the X-axis. The large delay prior to overspill after a −30°CA aTDC injection indicates a dependency on the ICP differential.

gas velocities creating low pressure around the orifice exit [66,67]. It is likely that internal pressure waves are also induced in the fluid residing within the closed channel i.e. the nozzle. The turbulence would explain the large spread of onset times between injections and orifices as the nearby pressures will greatly vary during both EOI and the overspill event. A trend for the onset times in regards to orifice position could not be found.

The ICP at the end of the injection may also impact the overspill phenomena. Swantek et al. and Kirsch et al. state that the primary cause of gas inside the nozzle is due to the ingestion of in-cylinder gas at the EOI [57,47]. During the EOI phase, fuel continues to exit the nozzle even after the needle valve closes. The in-nozzle space previously inhabited by the fuel is no longer refilled by fresh fuel from the body, creating a vacuum within the nozzle. The vacuum is equalised through the ingestion of in-cylinder gas, subsequently mixing with the residing in-orifice fuel. If the ingested gas is at an increased pressure when drawn into the orifice (as would be the case at TDC), the drop in in-cylinder pressure may cause greater expansion, thus a shorter injection-overspill delay and a greater volume of fuel release. This theory is supported by the overspill onset data (Fig. 9), in which the average overspill onset time when injecting at TDC (with high pressure ingested gas) is earlier than when injecting at −30°CA aTDC (with lower pressure ingested gas). Conversely, the average EOI-overspill delay from injecting at 30°CA aTDC is significantly less than that for the TDC injections, yet this is likely due to the greater pressure drop, superseding the influences of ingested gas pressure.

The overspill timing data obtained (Fig. 9) provides evidence that the majority of overspill events occur outside the period in which the film areas are measured between 6 and 18°CA aSOI. A few overspill events do occur within the processing period for TDC and 30°CA injection timings, yet they occur towards the end of this period. Considering that there is a short delay between the emergence of the fuel and the impact the overspill has on the film boundaries, it can be said that the overspill has a negligible influence over film behaviour during the period in which it has been measured. As a consequence, although the spreading rates may have clear dependencies on the in-cylinder conditions, the spreading rates are fundamentally due to spray wetting (the deposition of fuel during the dribble event) and its immediate spreading, rather than fuel emergence from within the nozzle.

4.2. The effect of injection duration on spray wetting

To ascertain the effects of injection duration and determine the degree of surface wetting occurring during the main injection phase, the evolution of coverage area for 4 injection durations (controlled via the trigger pulse widths) was investigated (Fig. 10). Since the pulse widths were varied from 0.2 to 1.0 ms, the EOI timing is not the same for all of the test-points giving a maximum difference of 0.8 ms (8 frames) between the falling edge times. All other operating conditions were kept constant for each test-point with a 50 MPa IP and TDC injection timing.

Films induced when using 0.2, 0.4 and 0.6 ms injection durations all showed similar behaviour and were rarely more than 1 standard deviation apart (Fig. 10). If a non-negligible amount of surface wetting occurred during the main injection phase, then a prolonged injection would increase the initial coverage area, resulting in consistently more wetting throughout the processing period. As this is not the case, it can be said that there is no wetting during the main injection phase. The fuel cannot splash back towards the nozzle or adhere to the surface since the high inertia of the emerging jet overcomes the influences of local gas interactions and jet turbulence that elicit the fuel deposition during the dribble event.

The films produced with 1 ms injection duration exhibited an average reduction of 71 % in coverage area and thus fuel deposition from the dribble event (Fig. 10). It is unlikely that the clear shift in behaviour of the 1 ms pulse width injections is anomalous as the standard deviation is also significantly smaller (despite an equivalent set size). This difference in initial wetting was also confirmed by visual inspection of the frames immediately after dispersion of the airborne droplets and vapour from injection (Fig. 11). A likely cause of the reduced coverage for the 1 ms injection is that a greater needle lift is reached for this pulse duration in comparison to the shorter duration injections [68].

To investigate this hypothesis the average mass flow rates from the injector were measured for 0.2 to 1.4 ms injection durations with a step of 0.2 ms. To obtain a pressure gradient across the orifice channel equivalent to 50 MPa IP injecting into the 5 MPa in-cylinder gas, the IP

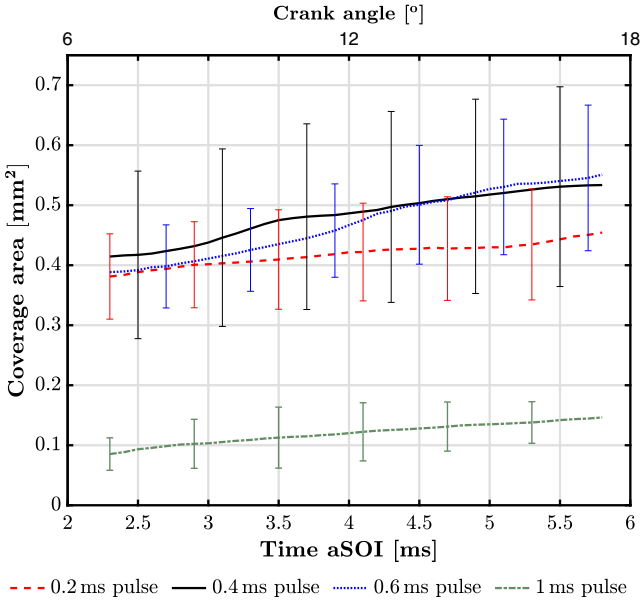

Fig. 10. Average temporal evolution of fuel coverage area as a function of time aSOI (50 MPa IP, TDC injection timing). The film evolutions for 0.2, 0.4 and 0.6 ms injection durations (trigger pulse widths) demonstrated similar behaviour, all within the ±1 standard deviation error bars. Films induced by the 1 ms duration injection presented considerable reductions in coverage areas.

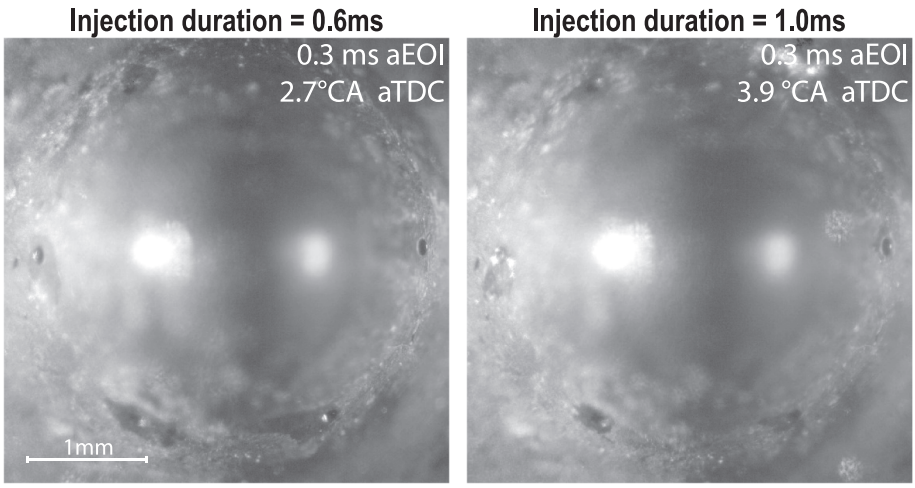

Fig. 11. The nozzle surface 0.3 ms aEOI demonstrating the difference in surface wetting when injecting at 0.6 ms (left) and 1 ms (right) duration. Both were injected at TDC with 50 MPa IP, yet there is a considerable reduction in film area when the duration is increased.

was set at 45 MPa (for injection into an ambient pressure vessel). One thousand injections were performed for each duration, after which the contents were weighed. The total mass was divided by the number of injections combined with the injection durations to acquire the average mass flow rate (Figs. 12 and 13). Measurements were performed in duplicates to obtain an uncertainty of ±0.65 g/s.

The mass flow significantly increases with respect to duration between 0.2 and 0.8 ms in a linear fashion, indicating that the flow is significantly throttled by the needle, thereby never achieving a stable internal flow pattern. A maximum mass flow is then reached for 0.8 ms injection duration. After this point, extending the duration gradually reduces the mass flow. An investigation that used the same injector type as ours supports the correlation, in which the measured needle lift does not reach its maximum at 40 MPa injection pressure and 1 ms injection duration [70]. The distinct difference in the differential of mass flow to duration suggests a considerable change to the internal flow pattern has occurred, potentially instigating stabilisation. Furthermore, the negative differential for flow rates above 0.8 ms implies that the prolonged injections elicit additional flow throttling. However, this throttling could not be induced via the needle since it would be at an identical or greater lift, so the throttling must result from another fluid dynamic process.

Winklhofer et al. performed investigations on flow through transparent, quasi two-dimensional orifices, analysing the mass flow and velocity field [69]. They found that as the flow inertia is increased beyond a critical point, the cavitation behaviour is significantly modified and the mass flow transitions from an inlet pressure dependency, to a dependency on the cavitation gas recirculation zones in the orifice channels. At this critical point, the recirculation zones considerably grow, greatly extending downstream of the orifice channel inlets. A venturi effect is applied to the flow path by the recirculation zones, reducing the streams diameter for a large section of the channel which keeps the flow rate relatively constant as the inlet pressure varies. It is believed that when the maximum needle lift is reached and the internal flow pattern stabilises, the resulting increase in orifice inlet pressure causes the same distinct change in cavitation behaviour that is described by Winklhofer et al., choking the flow and reducing the mass flow rate.

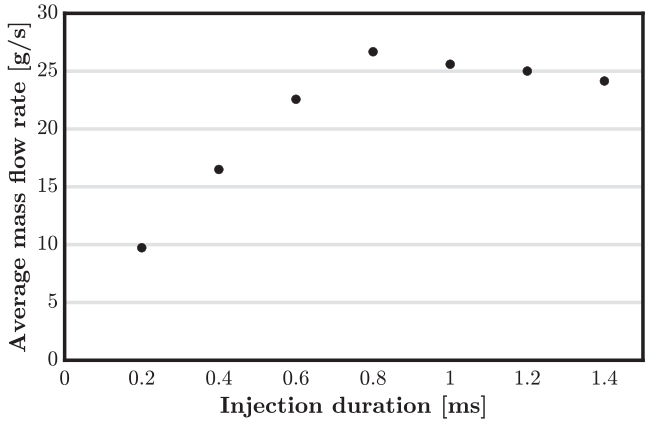

Fig. 12. Measured mass flow rates (in g/s) with respect to injection duration (in ms). The mass flow measurements are an average volume of 1000 injections at 45 MPa (into an ambient pressure vessel), divided by the duration. A considerable change occurs in the internal flow when injecting for longer than 0.8 ms after which a greater injection duration does not increase the flow rate, indicating choking of the flow through hydraulic behaviour [69].

Although the mass flow is reduced at longer injection durations, since the cavitation films reduce the effective diameter of the flow path, the flow still has greater fluid momentum on exiting the nozzle [71]. The higher inertia improved atomisation, reducing the size of the liquid structures at EOI, thus reducing susceptibility to the in-cylinder gas flow that potentially diverts the droplet trajectories back towards the nozzle surface. Higher flow exit velocities maintained for a prolonged duration helped induce a more stable external gas entrainment flow across the nozzle region, assisting in preventing fluid coverage. The flow stabilisation also dampens the turbulent behaviour within the nozzle and emerging EOI spray, decreasing the radial droplet velocities.

Additionally, Winklhofer et al. showed that the extended gas recirculation zones prevent the effects of the boundary layer in the periphery of the stream passing through the channel. Instead of velocities being considerably lower at the stream's periphery, compared to the central velocities, the fuel at the liquid–gas interface gains significantly higher velocities as the gas transfers additional momentum [69]. It is this fluid at the periphery of the stream, which would splash back onto the surface as it enters the cylinder, providing an explanation for the diminished wetting when this cavitation regime develops (Fig. 10).

In respect to the operating conditions studied, smaller injected mass (corresponding to the shorter injections) induced larger nozzle fuel films. This may suggest low load and idling engine operation are more susceptible to spray wetting, however high load conditions were not incorporated into the investigated operating points. At higher loads, greater gas densities, thermal expansion and vaporisation may dominate the processes discussed, impacting the trends observed at low to medium load.

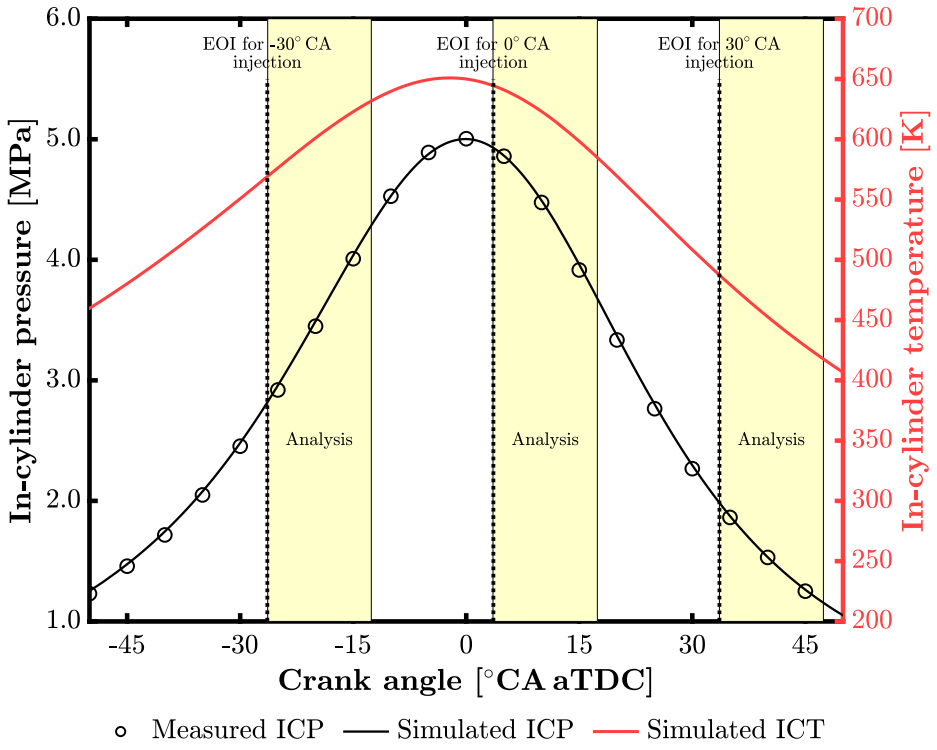

Fig. 13. The measured in-cylinder pressure supplemented by the approximated bulk gas pressures and temperatures simulated using a thermodynamic model. The similarity between the measured and simulated pressure gives confidence in the in-cylinder temperature data. The periods analysed using the image processing methods are also presented so that the instantaneous and differential in-cylinder conditions during these timings can be established.

4.3. The effect of ICP and ICT on spray wetting

A thermodynamic model was used to simulate the motored cycle and estimate the ICT. It performed calculations based on the known engine geometric parameters, the intake and the exhaust gas conditions with respect to the fundamental laws of thermodynamics. The equations incorporated the settings and known parameters in a system of differential equations then solved them through a variable order method (Matlab ODE113 solver [72,73]). The Hohenberg heat transfer correlation [74] was used to define the heat release term through a separate empiric equation [75]. Validation of the model was previously performed using laser induced grating spectroscopy [76,77]. The good agreement between the measured and simulated ICP suggests that the model is appropriately calibrated (Fig. 13) thus, the calculated bulk ICT is reasonable. The nozzle's subsurface temperature was also measured by a thermocouple embedded into the injector nozzle. The slow time constant of the thermocouple and large thermal inertia of the nozzle resulted in an average nozzle temperature of 405 ± 1 K, slightly higher than the average bulk gas temperature approximated by the model (over a full 360°CA cycle) of 384 ± 10 K.

By varying the injection timing between −30 and 30°CA, it was possible to create a wide range of conditions at the EOI and throughout the coverage area tracking period. Fig. 13 graphically displays the injection timings in terms of their EOI and corresponding processing periods with respect to the bulk ICP.

Fig. 14 shows the set-averaged coverage data for the conditions shown in Fig. 13, along with the corresponding trend lines and their equations. In consideration of the overspill onset times (Fig. 9) and the discussion found in Section 4.1, the evolution of coverage area given here is the spreading of fuel that was deposited through spray wetting at EOI with the influences of overspilling fuel shown to be negligible.

The rate at which the films spread across the nozzle are determined through the trend line gradients (Fig. 7 and Fig. 14), compared when varying the injection timing and pressure (Fig. 15). This decoupling of the film spreading rate enables segregation between the volume of fluid deposited at the EOI and the dynamics of the film after the EOI event. To approximate the initial deposition from spray wetting, the earliest reliable values of coverage area (2 ms aSOI) are also plotted with respect to IP and timing (Fig. 16). The correlating trends between the initial wetting and spreading rates suggest a direct relationship between the deposited volume and subsequent film motion (Fig. 15 and Fig. 16). It implies that the degree of fuel deposition is a primary factor in the subsequent spreading of the films. It also supports the previous statements that the film evolutions measured are not influenced by the overspill of fuel, else this relationship would be significantly impacted (Section 4.1).

Fig. 15 and Fig. 16 show that when injecting at TDC there is significantly more initial fuel deposition compared to injecting at ±30°CA for both IPs considered. At the instant of spray collapse when injecting at TDC, the increased ICP and corresponding density increase is expected to cause reduced momentum and penetration length in the dribbling fuel with a wider dispersion angle [78]. By decreasing the distance between the airborne droplets and nozzle surface, the chances of impingement will be considerably greater. There are also increased localised gas velocities due to turbulence created from the piston motion during this period, amplifying the interactions of the in-cylinder gas with any slow moving droplets [66,67]. These differences are expected to increase the likelihood of impingement from the EOI droplets and ligaments, leading to a greater volume of fuel adhering to the nozzle surface.

There is also significantly higher spreading rates when injecting near TDC (Figs. 15 and 14). This outcome may result purely from the strong relationship between initial deposition and spreading, yet there are several important factors which are likely to impact film spreading. ICT and ICP significantly increase during compression, peaking near TDC (Fig. 13). Higher ICP and ICT relax the contact angle and are conducive to more surface wetting through capillary action and reduced adhesive forces [79]. Given the timescales involved, it is likely that pressure would be the dominant effect since the thermal inertia in the nozzle tip

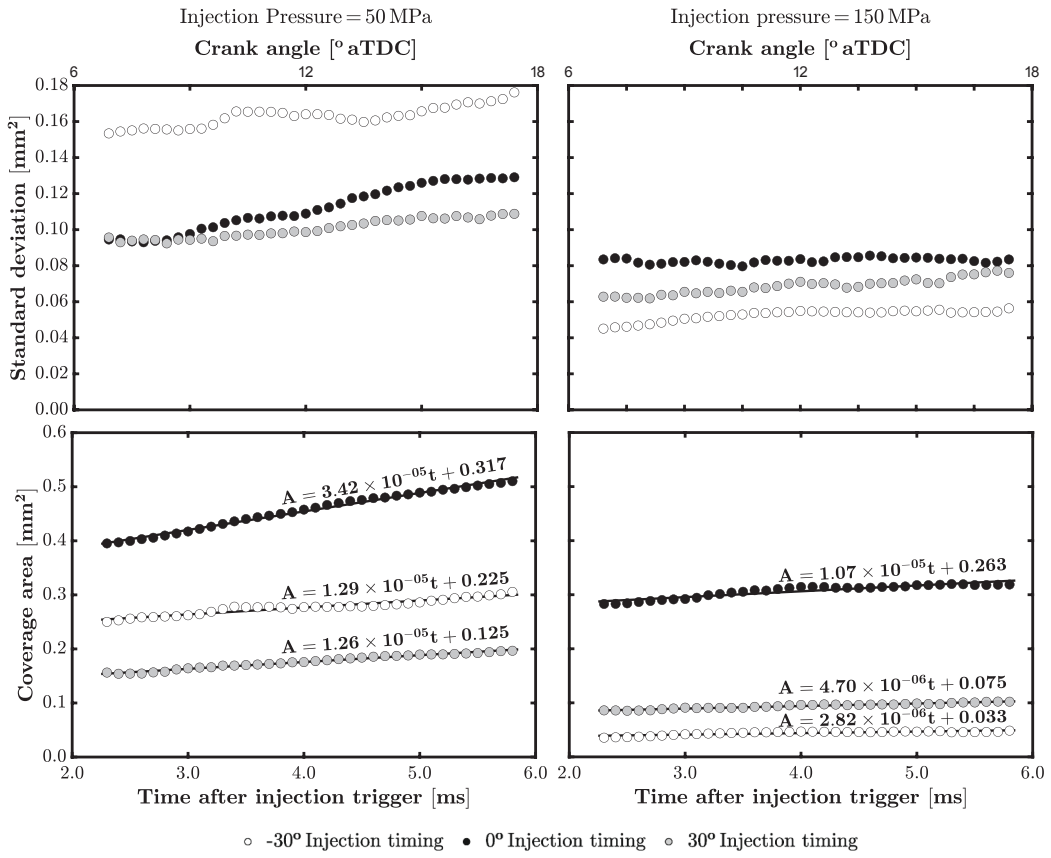

Fig. 14. Temporal evolution of set-averaged film coverage areas as a function of time aSOI. The left figure is for 50 MPa IP and the right is 150 MPa. −30°; 0°; +30°CA aTDC injection timings are plotted with the legend below. The solid lines are trend lines with their corresponding equations above, with A being the coverage area in mm^2 and t the time aSOI in milliseconds. The standard deviation of the sets are plotted separately above. The coverage area is consistently higher for 50 MPa IP and 0°CA injection timing.

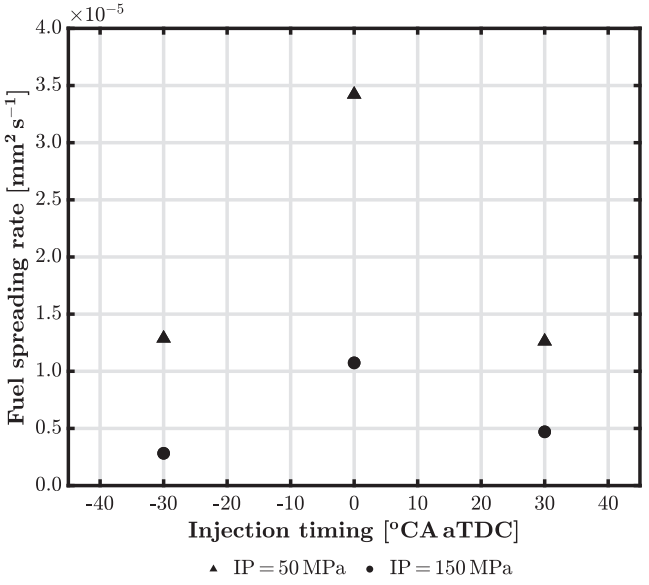

Fig. 15. The film spreading rates (trend line gradients in mm^{2}s^{-1}) when varying the injection timing (in °CA aTDC) and injection pressure (50 and 150 MPa). Injecting at TDC and increasing the injection pressure result in greater film spreading.

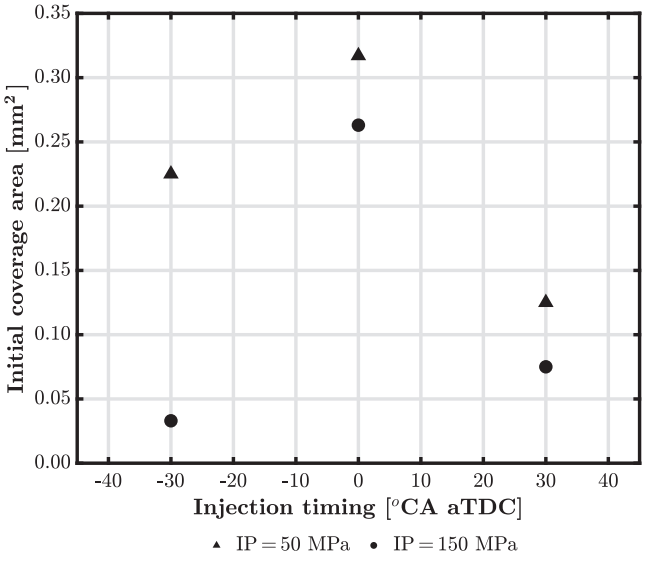

Fig. 16. The average coverage areas for each set taken at 2 ms aSOI, when the large droplets from the dribble event no longer impair the image processing measurements. They are plotted with respect to the injection timing and injection pressure. Strong correlation between spreading rate and initial wetting area demonstrates a primary dependency on the volume of fuel deposited during the dribble event.

will cause reduced temperature variation, yet the surface and gas temperatures may still provide some contribution. As discussed in the prior paragraph, the gas turbulence and density also increase which may amplify spreading if the gas interacts with the films.

4.4. The effect of injection pressure on spray wetting

Further investigation regarding the pressure gradient across the orifice channels were conducted through varying the IP between 50 and 150 MPa, resulting in more diverse ICP-IP gradients than those achieved from varying the injection timing alone. There is a clear trend in which increased IP causes considerable reductions to the coverage area for all injection timings (Figs. 15 and 16). The fuel has considerably more inertia on exiting the nozzle at increased IP, contracting the dispersion angle and increasing penetration at EOI [78]. By increasing the distance between the nozzle surface and injected fuel the likelihood of droplets impinging is significantly reduced. Moreover, the greater momentum of the fuel as the EOI phase finishes inhibits the fuel from adhering to the surface surrounding the injector. Atomisation will also increase, reducing number of large slow-moving droplets that potentially interact with the in-cylinder gas, splashing back toward the nozzle. In addition, the needle descent velocity is greater, reducing the time spent in the EOI phase.

As discussed in Section 4.2, Winklhoff et al. showed that at higher orifice inlet pressures an enhanced cavitation regime is achieved within the orifice channel [69]. The regime prevents the effects of the boundary layer on the flow creating increased inertia in the fluid on the periphery of the emerging jet. The fuel in the periphery of the jet has the highest likelihood of impinging on the surface due to the smaller separation from it. Since this regime is thought to be instigated by prolonged 50 MPa IP injections (Section 4.2), it almost certainly will occur for 150 MPa IP, likely to be a primary cause of the surface wetting reduction (Figs. 15 and 16).

All 50 MPa IP spray events exhibited surface wetting, yet several 150 MPa events did not. The absence of wetting events further supports the above statements indicating that increased flow exit velocities will inhibit the impingement and adherence of dribbling fuel. The data suggests that the low load/idling like conditions are more susceptible to the observed behaviour. However, greater thermal expansion and potential fuel vaporisation associated with higher loads may impact the trends observed. Additional research at high load conditions is recommended.

5. Conclusions

A realistic in-engine environment was replicated using an optically accessible reciprocating rapid compression machine and valve covered orifice type injector. A high-speed camera was employed with a long-distance microscope permitting visualisations of the near-nozzle and surface-bound fluid behaviour at the microscopic scale. Crank-resolved in-cylinder pressure measurements were obtained using an in-cylinder pressure sensor and the temperature field was established using a thermodynamic model and thermocouple embedded into the injector nozzle. Post-processing techniques were developed to track both the initial fuel coverage area on the nozzle surface, as well as the temporal evolution of surface-bound fluid. It was combined with a manual method for identification of the timings in which fuel first began emerging from within the nozzle. Through variation of the operating parameters the processes dictating spray wetting, its initial spreading and the late-cycle emergence of fuel were explored. The investigation led to the following conclusions:

- Spray wetting is negligible during the main injection phase due to the high inertia of the exiting fuel.
- Our findings indicate that greater injection pressures and durations induce a cavitation choked internal flow regime. The gas recirculation region within the orifice channel inhibits the boundary layer, increasing the liquid velocities on the periphery of the emerging liquid column and reducing EOI spray wetting. Low injection pressures (50 MPa) then increase the amount of fuel deposition due to EOI spray wetting. If the operating conditions reduce the axial fuel inertia during needle valve closing, there is a higher likelihood of the fuel either impinging or adhering to the external nozzle surface.
- The immediate spreading of spray deposited fuel is primarily dependent on the degree of fuel initially deposited, rather than on the in-cylinder gas conditions. However, the degree of EOI spray wetting increases when injecting into a higher pressure gas due to greater turbulence and dispersion angles.
- The overspill events are strongly dependent on the drop in in-cylinder pressure during the expansion stroke, indicating that the expansion of orifice trapped gas dislodging the residing in-orifice fuel is the primary contributor.

It should be noted that these results are specific to convergent VCO type nozzles, and further investigations are required for sac type nozzles. The data is presented in terms of film area, thus the conclusions must be further validated by quantification of the film volume. Film thickness measurements, permitting volumetric analyses, are potentially achievable by incorporating multi-dye fluorescence techniques [80].

CRediT authorship contribution statement

Dan Sykes: Writing - original draft, Methodology, Software, Validation, Visualization. **Jack Turner:** Investigation, Writing - review & editing. **Viacheslav Stetsyuk:** Investigation, Writing - review & editing. **Guillaume Sercey:** Software, Writing - review & editing. **Martin Gold:** Funding acquisition, Writing - review & editing, Project administration. **Richard Pearson:** Funding acquisition, Project administration. **Cyril Crua:** Conceptualization, Funding acquisition, Supervision, Visualization, Writing - review & editing.

Declaration of Competing Interest

The authors declare that they have no known competing financial interests or personal relationships that could have appeared to influence the work reported in this paper.

Acknowledgements

This work was supported by the UK's Engineering and Physical Science Research Council [EPSRC grants EP/K020528/1 and iCASE Studentship 1793447] and BP International Ltd.

Appendix A. Supplementary data

Supplementary data associated with this article can be found, in the online version, at https://doi.org/10.1016/j.fuel.2020.119833.

References

[1] Höök M, Tang X. Depletion of fossil fuels and anthropogenic climate change—a review. Energy Policy 2013;52:797–809. https://doi.org/10.1016/j.enpol.2012.10.046. ISSN 0301-4215.
[2] Koci CP, Fitzgerald RP, Ikonomou V, Sun K. The effects of fuel–air mixing and injector dribble on diesel unburned hydrocarbon emissions. Int J Engine Res 2019;20(1):105–27. https://doi.org/10.1177/1468087418821827. ISSN 1468-0874.
[3] Mohammed MK, Rahman M, Bakar RA. Effects of air-fuel ratio and engine speed on performance of hydrogen fueled port injection engine, vol. 9; 2009. doi: 10.3923/jas.2009.1128.1134.
[4] Dec JE. A conceptual model of DI diesel combustion based on laser-sheet imaging. SAE Int 1997. https://doi.org/10.4271/970873.
[5] Taskinen P. Effect of fuel spray characteristics on combustion and emission formation in a large medium speed diesel engine. SAE Int 1998. https://doi.org/10.4271/982583.

[6] Zhu J, Kuti OA, Nishida K. Effects of injection pressure and ambient gas density on fuel – ambient gas mixing and combustion characteristics of D.I. diesel spray. SAE Int 2011. https://doi.org/10.4271/2011-01-1819.

[7] Koci C, Dempsey A, Nudd J, Knier B. Understanding hydrocarbon emissions in heavy duty diesel engines combining experimental and computational methods. SAE Int J Engines 2017;10(3):1093–109. https://doi.org/10.4271/2017-01-0703.

[8] Fanick R, Kroll S. Semi-volatile organic compounds from a combined dual port injection/direct-injection technology light-duty gasoline vehicle ISSN 0148-7191. doi: 10.4271/2019-24-0051.

[9] Som S, Ramirez AI, Longman DE, Aggarwal SK. Effect of nozzle orifice geometry on spray, combustion, and emission characteristics under diesel engine conditions. Fuel 2011;90(3):1267–76. https://doi.org/10.1016/j.fuel.2010.10.048.

[10] D. T. delphi diesel common rail systems, DFI21 injectors: heavy-duty pressure relief, Report, URL www.delphi.com/innovations/dfi21-injectors-heavy-duty-pressure-relief#, 2018.

[11] Matsumoto S, Yamada K, Date K. Concepts and evolution of injector for common rail system. SAE Int 2012. https://doi.org/10.4271/2012-01-1753.

[12] Bergstrand P, Denbratt I. Diesel combustion with reduced nozzle orifice diameter. SAE Int 2009. https://doi.org/10.4271/2001-01-2010.

[13] Lingens A, Senghaas C, Willmann M, Schneider H. Next generation of smart injectors for future diesel and dual-fuel applications. In: Siebenpfeiffer W, editor, Heavy-duty-, on- und off-highway-motoren 2018; 2019. 377-391ISSN 978-3-658-25888-7, doi: 10.1007/978-3-658-25889-4_22.

[14] Tree DR, Svensson KI. Soot processes in compression ignition engines. Prog Energy Combust Sci 2007;33(3):272–309. https://doi.org/10.1016/j.pecs.2006.03.002. ISSN 0360-1285.

[15] Barker J, Richards P, Goodwin M, Wooler J. Influence of high injection pressure on diesel fuel stability: a study of resultant deposits. SAE Int J Fuels Lubric 2009;2(1):877–84. https://doi.org/10.4271/2009-01-1877.

[16] Alves Fortunato M, Lenglet F, Ben Amara A, Starck L. Are internal diesel injector deposits (IDID) mainly linked to biofuel chemical composition or/and engine operation condition? In: SAE Technical Paper Series; 2019. doi: 10.4271/2019-01-0061.

[17] Knorsch T, Rogler P, Miller M, Wiese W. On the evaluation methods for systematic further development of direct-injection nozzles. SAE Int 2016. https://doi.org/10.4271/2016-01-2200.

[18] Johansson AN, Dahlander P. Experimental investigation on the influence of boost on emissions and combustion in an SGDI-engine operated in stratified mode. In: SAE Technical Paper Series; 2015. doi: 10.4271/2015-24-2433.

[19] Sjöberg M, Dec JE. Combined effects of fuel-type and engine speed on intake temperature requirements and completeness of bulk-gas reactions for HCCI combustion. SAE Int 2003. https://doi.org/10.4271/2003-01-3173.

[20] Han S, Bae C. The influence of fuel injection pressure and intake pressure on conventional and low temperature diesel combustion. SAE Int 2012. https://doi.org/10.4271/2012-01-1721.

[21] Birgel A, Ladommatos N, Aleiferis P, Zülch S, Milovanovic N, Lafon V, et al. Deposit formation in the holes of diesel injector nozzles: a critical review. In: Powertrains, fuels & lubricants meeting, Rosemont, USA; 2008. doi: 10.4271/2008-01-2383, October 6–9.

[22] Caprotti R, Breakspear A, Graupner O, Klaua T. Detergency requirements of future diesel injection systems. In: Powertrain & fluid systems conference & exhibition, San Antonio (TX), USA; October 24–27, 2005. doi: 10.4271/2005-01-3901.

[23] Reid J, Cook S, Barker J. Internal injector deposits from sodium sources. SAE Int J Fuels Lubric 2014;7(2):436–44. https://doi.org/10.4271/2014-01-1388.

[24] Barker J, Richard P, Snape C, Meredith W. Diesel injector deposits – an issue that has evolved with engine technology. SAE Int 2011. https://doi.org/10.4271/2011-01-1923.

[25] Magno A, Mancaruso E, Vaglieco BM, Florio S, Gioco G, Rebesco E. Study on spray injection and combustion of fouled and cleaned injectors by means of 2D digital imaging in a transparent CR diesel engine. SAE Int 2013. https://doi.org/10.4271/2013-24-0062.

[26] Cracknell R, Wardle R, Pos R, Ganippa L. Effect of diesel injector tip deposits on transient spray behavior. In: Liebl J, Beidl C, editors. Internationaler motorenkongress 2016, Springer Fachmedien Wiesbaden, 185–193; 2016, doi: 10.1007/978-3-658-12918-7_13.

[27] Ym A, Furuhata T, Saito M, Arai M. Diesel and bio-diesel fuel deposits on a hot surface. Fuel 2008;87:1601–9. https://doi.org/10.1016/j.fuel.2007.07.030.

[28] Güralp O. The effect of combustion chamber deposits on heat transfer and combustion in a homogeneous charge compression ignition engine https://deepblue.lib.umich.edu/handle/2027.42/58488.

[29] Weidenlener A, Pfeil J, Kubach H, Koch T, Forooghi P, Frohnapfel B, Magagnato F. The influence of operating conditions on combustion chamber deposit surface structure, deposit thickness and thermal properties. Autom Engine Technol 2018;3(3):111–27. https://doi.org/10.1007/s41104-018-0030-3. ISSN 2365-5135.

[30] Khan M, Khan M, Shakoor DA. A failure analysis of the exhaust valve from a heavy duty natural gas engine. Eng Failure Anal 85. doi: 10.1016/j.engfailanal.2017.12.001.

[31] Wang Y. Study of deposit formation inside diesel injectors nozzles. Thesis; 2011. doi: 1721.1/79512.

[32] Fischer A, Thelliez M. Methodology and tools to predict GDI injector tip wetting as predecessor of tip sooting. SAE Int 2018. https://doi.org/10.4271/2018-01-0286.

[33] Birgel A, Ladommatos N, Aleiferis P, Milovanovic N, Lacey P, Richards P. Investigations on deposit formation in the holes of diesel injector nozzles. SAE Int J Fuels Lubric 2011;5(1):123–31. https://doi.org/10.4271/2011-01-1924. ISSN 1946-3960.

[34] Caprotti R, Bhatti N, Balfour G. Deposit control in modern diesel fuel injection systems. SAE Int J Fuels Lubric 2010;3(2):901–15. https://doi.org/10.4271/2010-01-2250.

[35] Rounthwaite N, McGilvery C, Jiang J, Williams R, Giuliani F, Britton T. A chemical and morphological study of diesel injector nozzle deposits – insights into their formation and growth mechanisms, in: SAE 2017 world congress and exhibition, vol. 10, SAE International, 106–114; 2017. doi: 10.4271/2017-01-0798.

[36] Lacey P, Gail S, Kientz JM, Milovanovic N, Gris C. Internal fuel injector deposits. doi: 10.4271/2011-01-1925.

[37] Lacey P, Gail S, Kientz JM, Benoist G, Downes P, Daveau C. Fuel quality and diesel injector deposits. doi: 10.4271/2012-01-1693.

[38] Slavchov RI, Mosbach S, Kraft M, Pearson R, Filip SV. An adsorption-precipitation model for the formation of injector external deposits in internal combustion engines. Appl Energy 2018;228:1423–38. https://doi.org/10.1016/j.apenergy.2018.06.130. ISSN 0306-2619.

[39] Turner JE, Stetsyuk V, Crua C, Pearson RJ, Gold MR. The effect of operating conditions on post-injection fuel discharge in an optical engine. In: ICLASS 13th triennial international conference, Tainan, Taiwanl; August 23–27, 2015. http://ilasseurope.org/events/13th-iclass-2015/.

[40] Leick P, Bork B, Geiler JN. Experimental characterization of tip wetting in gasoline DI injectors. In: ICLASS 2018, 14th triennial international conference on liquid atomization and spray systems; 2018. URL www.researchgate.net/profile/Philippe_Leick/publication/326583778.

[41] Eagle WE. Cinema-stereo imaging of fuel dribble after the end of injection in an optical heavy-duty diesel engine. In: THIESEL conference on thermo- & fluid dynamic processes in direct injection engines, Valencia, Spain; September 9–12, 2014. https://www.tib.eu/en/search/id/TIBKAT%3A495266671/Conference-proceedings-THIESEL-2004-Conference/.

[42] Gold M, Pearson R, Turner J, Sykes D, Stetsyuk V, de Sercey G, Crua C, Murali-Girija M, Koukouvinis F, Gavaises M. Simulation and measurement of transient fluid phenomena within diesel injection. SAE Int 2019. https://doi.org/10.4271/2019-01-0066.

[43] Duleep KG. The impact of gasoline direct injection system design on PM emissions. In: SAE Technical Paper Series; 2019. doi: 10.4271/2019-01-0072.

[44] Jafarmadar S. The effect of split injection on the combustion and emissions in DI and IDI diesel engines, diesel engine – combustion, emissions and condition monitoring. ISSN 978-953-51-1120-7, doi: 10.5772/55232.

[45] Shangar Ramani V, Muthusamy A, Bhachchu G. Reduction of diesel engine combustion noise through various injection strategies. SAE Int 2019. https://doi.org/10.4271/2019-26-0211.

[46] Lundgren MO, Wang Z, Matamis A, Andersson O, Richter M, Tuner M, Alden M, Arne A. Effects of post-injections strategies on UHC and CO at gasoline PPC conditions in a heavy-duty optical engine. SAE Int 2017. https://doi.org/10.4271/2017-01-0753.

[47] Kirsch V, Reddemann MA, Palmer J, Kneer R. Zooming into primary breakup mechanisms of high-pressure automotive sprays. In: ILASS–Europe 2017, 28th conference on liquid atomization and spray systems; 2017. doi: 10.4995/ILASS2017.2017.4603.

[48] Fitzgerald RP, Bazyn T. Dribble quantification for diesel fuel injectors. In: ICLASS 2018, 14th triennial international conference on liquid atomization and spray systems; 2018. URL www.iclass2018.org/program/s204.html.

[49] Zhou J, Zhang Y, Qin J, Liu C, Wang L, Han X, Pei Y, Zhan ZS, Wu X, Hu TG, Su X, Zhang C, Chen T. An investigation of abnormal spray behaviors of multi-hole GDI injector. SAE Int 2016. https://doi.org/10.4271/2016-01-0848.

[50] Sechenyh V, Duke DJ, Swantek AB, Matusik KE, Kastengren AL, Powell CF, Viera A, Payri R, Crua C. Quantitative analysis of dribble volumes and rates using three-dimensional reconstruction of X-ray and diffused back-illumination images of diesel sprays. Int J Engine Res 2019;21(1):43–54. https://doi.org/10.1177/1468087419860955. ISSN 1468-0874.

[51] Koci C, Martin G, Bazyn T, Morrison W, Svensson K, Gehrke C. The influence of diesel end-of-injection rate shape on combustion recession. SAE Int J Engines 2015;8(2):647–59. https://doi.org/10.4271/2015-01-0795. ISSN 1946-3944.

[52] Pos R, Avulapati MM, Wardle R, Cracknell R, Megaritis T, Ganippa L. Combustion of ligaments and droplets expelled after the end of injection in a multi-hole Diesel injector, vol. 197; 2017. doi: 10.1016/j.fuel.2017.02.048.

[53] Arsie I, Di Leo R, Pianese C, De Cesare M. Enhanced combustion model with fuel-wall impingement oriented to injection pattern tuning in automotive diesel engines. IFAC-PapersOnLine 2016;49(11):476–83. https://doi.org/10.1016/j.ifacol.2016.08.070. ISSN 2405-8963.

[54] Xu H, Wang C, Ma X, Sarangi AK, Weall A, Krueger-Venus J. Fuel injector deposits in direct-injection spark-ignition engines. Prog Energy Combust Sci 50 (C): 2015;63–80. doi: 10.1016/j.pecs.2015.02.002, ISSN 0360-1285.

[55] Arifin YM, Furuhata T, Saito M, Arai M. Diesel and bio-diesel fuel deposits on a hot surface. Fuel 2008;87(8):1601–9. https://doi.org/10.1016/j.fuel.2007.07.030. ISSN 0016-2361.

[56] Pos R. Spatio-temporal evolution of diesel sprays using high-speed optical diagnostics, Thesis, URL http://bura.brunel.ac.uk/handle/2438/14481, 2016.

[57] Swantek A, Duke D, Sovis N. End of injection, mass expulsion behaviors in single hole diesel fuel injectors. In: Proceedings of ILASS Americas, Portland (OR), USA; September 18–21, 2014a. http://www.ilass.org/ilassOrgPortal-Americas.htm.

[58] Swantek AB, Kastengren AL, Duke D, Tilocco FZ, Sovis N, Powell CF. A further examination of fuel dribble from single hole diesel nozzles. In: ILASS-Europe 26th annual conference on liquid atomization & spray systems, Bremen, Germany; September 8–10, 2014b. http://ilasseurope.org/publications/proceedings/.

[59] Papadopoulos N, Aleiferis P. Numerical modelling of the in-nozzle flow of a diesel injector with moving needle during and after the end of a full injection event. 12th

International conference on engines & vehicles 2015;8(5):2285–302. https://doi.org/10.4271/2015-24-2472.
[60] Battistoni M, Xue Q, Som S. Large-Eddy simulation (LES) of spray transients: start and end of injection phenomena. Oil Gas Sci Technol-Revue d'IFP Energies nouvelles 2015;71(1):1–4. https://doi.org/10.2516/ogst/2015024.
[61] Battistoni M, Poggiani C, Som S. Prediction of the nozzle flow and jet characteristics at start and end of injection: transient behaviors. SAE Int J Engines 2015;9(1):84–97. https://doi.org/10.4271/2015-01-1850.
[62] Caprotti R, Fowler WJ, Lepperhoff G, Houben M. Diesel additive technology effects on injector hole erosion/corrosion, injector fouling and particulate traps. In: SAE international fuels & lubricants meeting & exposition, Philadelphia, Pennsylvania; October 18-21, 1993. doi: 10.4271/932739.
[63] Yu RC, Kuo TW, Shahed SM, Chang TW. The effect of mixing rate, end of injection, and sac volume on hydrocarbon emissions from a D.I. diesel engine. SAE Int 1983. https://doi.org/10.4271/831294.
[64] Crua C. Combustion processes in a diesel engine, Ph.D. thesis, University of Brighton, Brighton, UK, URL http://eprints.brighton.ac.uk/1161/, 2002.
[65] Sykes D, de Sercey G, Gold M, Pearson R, Crua C. Visual analyses of end of injection liquid structures and the behaviour of nozzle surface-bound fuel in a direct injection diesel engine. In: International powertrains, fuels and lubricants meeting. doi: 10.4271/2019-01-0059, 2019, ISSN 0148-7191.
[66] Bozza F, Bellis VD, Berni F, D'adamo A., Maresca L. Refinement of a 0D turbulence model to predict tumble and turbulent intensity in SI engines. Part I: 3D analyses. SAE Int; 2018. doi: 10.4271/2018-01-0850.
[67] Rota C, Morgan R, Osborne R, Mason D, Heikal M, Matrisciano A, Mustafa K. A process for an efficient heat release prediction at multiple engine speeds and valve timings in the early stage of gasoline engine development. SAE Int. doi: 10.4271/2019-24-0085, 2019, ISSN 0148-7191.
[68] Lockett R, Jeshani M, Makri K, Price R. An optical characterization of atomization in non-evaporating diesel sprays. SAE Int 2016. https://doi.org/10.4271/2016-01-0865.
[69] Winklhofer E, Kull E, Kelz E, Morozov A. Comprehensive hydraulic and flow field documentation in model throttle experiments under cavitation conditions. in: ILASS-Europe, editor. ILASS-Europe 2001, 17 international conference on liquid atomization and spray; 2001. doi: 10.13140/2.1.1716.4161.
[70] Punov P. Research the fuel injection characteristics of a common-rail solenoid injector. In: BulTrans, 153–158, URL www.researchgate.net/publication/309813548_Research_the_fuel_injection_characteristics_of_a_common-rail_solenoid_injector, 2015.
[71] Sazhin S, Crua C, Kennaird D, Heikal M. The initial stage of fuel spray penetration. Fuel 2003;82(8):875–85. https://doi.org/10.1016/S0016-2361(02)00405-2.
[72] Shampine LF, Gordon MK. Computer solution of ordinary differential equations: the initial value problem, San Francisco: W. H. Freeman, ISBN: 0716704617, 1975.
[73] Shampine LF, Reichelt MW. The MATLAB ODE suite. SIAM J Sci Comput 1997;18(1):1–22. https://doi.org/10.1137/s1064827594276424.
[74] Hohenberg GF. Advanced approaches for heat transfer calculations. SAE Int 1979. https://doi.org/10.4271/790825.
[75] Soyhan HS, Yasar H, Walmsley H, Head B, Kalghatgi GT, Sorusbay C. Evaluation of heat transfer correlations for HCCI engine modeling. Appl Therm Eng 2009;29(2):541–9. https://doi.org/10.1016/j.applthermaleng.2008.03.014. ISSN 1359-4311.
[76] Förster F, Crua C, Davy M, Ewart P. Temperature measurements under diesel engine conditions using laser induced grating spectroscopy. Combust Flame 2019;199:249–57. https://doi.org/10.1016/j.combustflame.2018.10.017. ISSN 0010-2180.
[77] Förster FJ, Crua C, Davy M, Ewart P. Time-resolved gas thermometry by laser-induced grating spectroscopy with a high-repetition rate laser system. Exp Fluids 2017;58(7):87. https://doi.org/10.1007/s00348-017-2370-6. ISSN 1432-1114.
[78] Siebers DL. Scaling liquid-phase fuel penetration in diesel sprays based on mixing-limited vaporization, 1999. doi: 10.4271/1999-01-0528, l349 SAE Technical Paper 1999-01-0528.
[79] Caudwell DR, Trusler JPM, Vesovic V, Wakeham WA. The viscosity and density of n-dodecane and n-octadecane at pressures up to 200 MPa and temperatures up to 473 K. Int J Thermophys 2004;25(5):1339–52. https://doi.org/10.1007/s10765-004-5742-0. ISSN 1572-9567.
[80] Brend MA, Barker AG, Carrotte JF. Measurements of fuel thickness for prefilming atomisers at elevated pressure. Int J Multiphase Flow 2020;131:103–313. https://doi.org/10.1016/j.ijmultiphaseflow.2020.103313. ISSN 0301-9322.